Comprehensive transport study of anisotropy and ordering phenomena in quasi-one-dimensional $(TMTTF)_2X$ salts ($X = PF_6, AsF_6, SbF_6, BF_4, ClO_4, ReO_4$)

B. Köhler, E. Rose, M. Dumm, G. Untereiner, and M. Dressel
Physikalisches Institut, Universität Stuttgart, Pfaffenwaldring 57, D-70550 Stuttgart, Germany
(Received 11 November 2010; revised manuscript received 21 March 2011; published 26 July 2011)

The temperature-dependent dc resistivity of the quasi-one-dimensional organic salts $(TMTTF)_2X$ ($X = PF_6, AsF_6, SbF_6, BF_4, ClO_4, ReO_4$) [tetramethyltetrathiafulvalene (TMTTF)] has been measured in all three crystal directions in order to investigate anisotropy, localization effects, and charge- (CO) and anion-ordering (AO) phenomena at low temperatures. For all compounds and directions, we extract the transport mechanisms in different regimes. The data are thoroughly analyzed, related to structural properties, and extensively discussed in view of previous studies and latest theories. The most important observation is the opening of a gap in the density of states below the CO temperature T_{CO} that influences the transport in all three directions. The effect becomes stronger as the distance between the anions and the sulfur atoms decreases. The coupling between the anions and the TMTTF stack also has a strict influence on the anomaly in the resistivity at the AO T_{AO}. At very low temperatures, the activation law is replaced by three-dimensional variable-range hopping.

DOI: 10.1103/PhysRevB.84.035124 PACS number(s): 71.30.+h, 74.70.Kn, 71.27.+a, 72.15.−v

I. INTRODUCTION

For the last half century, organic conductors have been established as models to investigate the physics in reduced dimensions.[1] In a one-dimensional electron gas, for instance, Fermi-liquid theory breaks down, and spin and charge degrees of freedom become separated.[2] But the metallic phase of a solid is not stable in one dimension: As the temperature is reduced, the electronic charges and spins tend to arrange themselves in an orderly fashion due to strong correlations. The competition among the different interactions upon the charge, the spin, and the lattice degrees of freedom is responsible for which broken-symmetry ground state is eventually realized in a specific compound.[3]

The Fabre salts $(TMTTF)_2X$ [tetramethyltetrathiafulvalene (TMTTF)] are charge-transfer salts consisting of stacks of the planar organic molecules TMTTF along the a axis that are separated in the c direction by monovalent anions. In the b direction, the distance of the stacks is comparable to the van der Waals radii. In the case of the Bechgaard salts, the tetramethyltetraselenafulvalene (TMTSF) molecule contains selenium instead of sulfur with more extended orbitals.

According to stoichiometry, $(TMTCF)_2X$ salts should form metallic compounds with a three-quarter-filled conduction band, but due to their strong anisotropy and electronic interaction, most of the systems become insulating upon cooling. What was considered to be disappointing at the beginning, in fact, contained the most exciting physics: The families of the Fabre and Bechgaard salts have been in the focus of enormous scientific effort during the last three decades because small variations in the molecules or moderate pressure tune the systems through several interesting ground states, such as an antiferromagnetic (AFM) insulator, a spin-Peierls state, a spin-density-wave state, and a superconductor, furthermore, one observes a crossover from a Luttinger liquid toward a Fermi-liquid metal, a charge-ordered (CO) insulator, and the electronic ferroelectrics.[4–8]

While theoretical models commonly start in strictly one dimension, real TMTSF and TMTTF salts exhibit a certain interchain coupling that has a strict influence on the physical properties. In addition, it turns out that the anions do not simply act as a charge reservoir and a spacer, but their interaction with the organic molecules is crucial for the low-temperature properties of these materials. The understanding of the different amounts of charge localization in the Fabre TMTTF salts and the effects of CO and anion ordering (AO) requires reliable information on the transport properties along the different directions. Although various groups performed numerous studies along the stacking direction, only little is known in the perpendicular direction. Here, we present the temperature-dependent dc resistivity in all three directions of the quasi-one-dimensional organic salts $(TMTTF)_2X$ containing anions of octahedral ($X = PF_6$, AsF_6, and SbF_6) and tetrahedral symmetry ($X = BF_4$, ClO_4, and ReO_4). The findings are compared with literature data and are discussed according to the latest theory.

II. EXPERIMENTAL DETAILS

Single crystals of $(TMTTF)_2X$ with $X = PF_6$, AsF_6, SbF_6, BF_4, ClO_4, ReO_4 were grown by electrochemical methods in an H-type glass cell at room temperature. A constant voltage of 1.5 V was applied between platinum electrodes with an area of approximately 3 cm^2. The current through the solution was between 9.2 and 13.4 μA. To reduce the diffusion, a sand barrier was introduced. After several months, we were able to harvest needle-shaped single crystals of several millimeters in length and less than a millimeter in width. All compounds of the TMTTF family are isostructural. Due to the triclinic symmetry, b' denotes the projection of the b axis perpendicular to a, and c^* is normal to the ab plane.

In order to measure the dc resistivity, small gold contacts were evaporated onto the natural crystal surface, and thin gold wires were attached by carbon paste. Along the long a axis of the crystals and also for the b' direction, four-point measurements could be performed, while for the c^* direction, two contacts were applied on opposite sides of the crystal. The

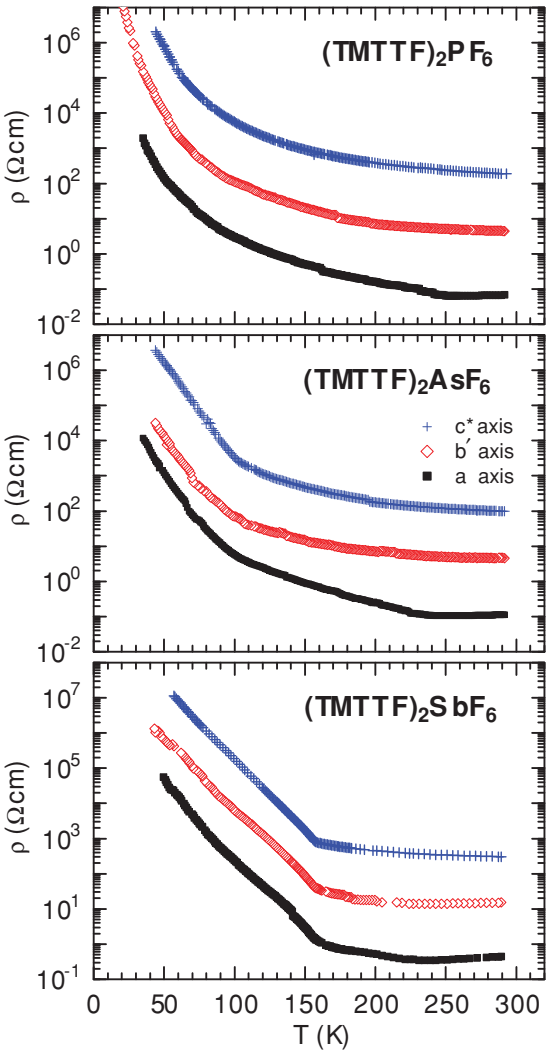

FIG. 1. (Color online) Temperature dependence of the dc resistivity in $(TMTTF)_2X$ crystals with octahedral anions $X = PF_6$, AsF_6, and SbF_6 along the three crystal directions a, b', and c^*.

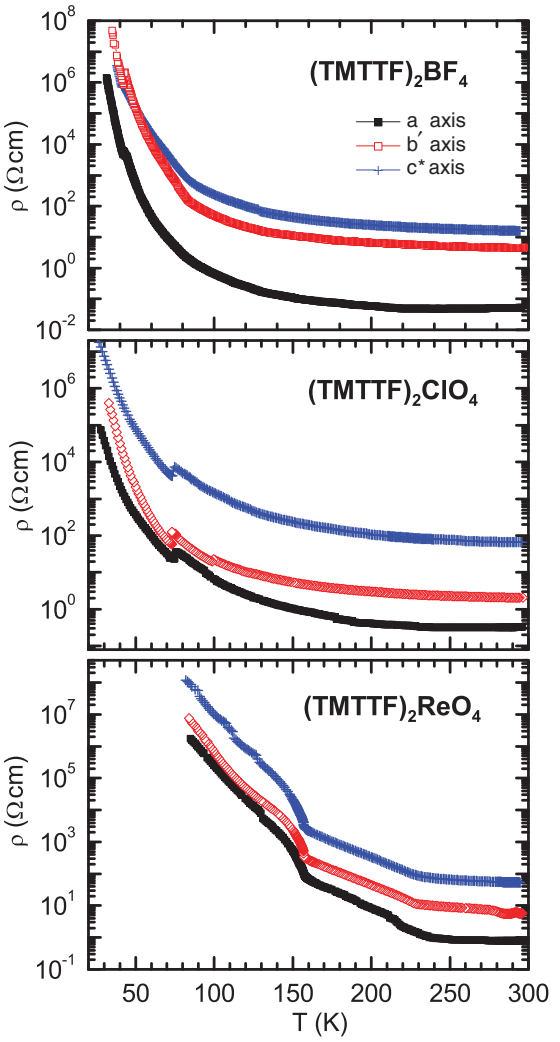

FIG. 2. (Color online) Temperature-dependent dc resistivity of $(TMTTF)_2X$ crystals with thetrahedal anions $X = BF_4$, ClO_4, and ReO_4 along the three directions a, b', and c^*.

samples were attached to a sapphire plate in order to ensure good thermal contact and were cooled down slowly to helium temperatures.

III. RESULTS

In Fig. 1, the temperature-dependent dc resistivity of different TMTTF salts with centrosymmetric anions PF_6, AsF_6, and SbF_6 is plotted in a logarithmic fashion to show the overall behavior. The measurements have been performed along the principal directions a, b', and c^*. The results for compounds with tetrahedral anions $X = BF_4$, ClO_4, and ReO_4 are presented in Fig. 2. The observed temperature dependences are in good accord among different batches and with previous reports.

The absolute values of the room-temperature resistivity ρ_a do not differ much for the various compounds. They range from 0.05 Ω cm for $(TMTTF)_2BF_4$ to 0.8 Ω cm for $(TMTTF)_2ReO_4$ and are listed in Table I. The wide spread of values reported in literature[9–12] can be ascribed to for a number of reasons: the way contacts are attached, how the current is injected, how the influence of microcracks is corrected for, and (maybe for the least extent) the quality of the crystals. In our studies, we applied a consistent procedure for all specimens that ensured a solid basis for comparison.

For very anisotropic samples, it poses a challenge to measure only the contributions along the chains because strands might be broken and the chains might contain defects or other

TABLE I. Room-temperature dc resistivity ρ_a and anisotropy of $(TMTTF)_2X$ for different anions $X = PF_6$, AsF_6, SbF_6, BF_4, ClO_4, and ReO_4.

	$(TMTTF)_2X$					
X	ρ_a (Ω cm)	ρ_a	/	$\rho_{b'}$	/	ρ_{c^*}
PF_6	0.08	1		50		2000
AsF_6	0.2	1		30		1000
SbF_6	0.4	1		40		600
BF_4	0.05	1		88		303
ClO_4	0.3	1		4		120
ReO_4	0.8	1		7		70

imperfections. The one-dimensional TMTSF and TMTTF salts are generally known to be particularly susceptible to cracks during cooling. Thus, to some extent, the electrical properties along the a direction may be effected by the b'- and c^*-axes transport. Nevertheless, since the same overall behavior was repeatedly observed in numerous specimens, we could identify intrinsic properties, including similar transport mechanisms and ordering phenomena in all three directions. Applying the same procedure to all samples yields consistent results and allows for comparison between different compounds.

A. Anisotropy

It is remarkable that, for all investigated $(TMTTF)_2X$ compounds, the temperature-dependent resistivity in many regards shows a similar temperature behavior for the three directions. The overall evolution of $\rho_a(T)$, $\rho_{b'}(T)$, and $\rho_{c^*}(T)$ with temperature behavior roughly differs by a constant factor (i.e., parallel to one another in the logarithmic representation), and the signatures of the ordering transitions are distinctly pronounced not only along the stacking direction, but also in $\rho_{b'}(T)$ and $\rho_{c^*}(T)$ as well. Upon lowering the temperature, the anisotropy in all compounds slightly decreases for $T < 230$ K, i.e., in the temperature range where in some way, transport is activated thermally.

For the three compounds with centrosymmetric anions $X = PF_6$, AsF_6, and SbF_6, the anisotropy $\rho_{b'}/\rho_a$ is approximately 30–50, and $\rho_{c^*}/\rho_a \approx 10^3$. Notably, for the group of compounds with noncentrosymmetric anions ($X = BF_4$, ClO_4, and ReO_4), the anisotropy is, in general, lower. In Table I, the room-temperature resistivity anisotropy $\rho_a/\rho_{b'}/\rho_{c^*}$ is listed for all compounds under investigation.

B. Localization and ordering phenomena

At high temperatures, basically all investigated compounds develop a metal-like behavior for transport along the a direction down to a localization temperature T_ρ. In addition, the ordering phenomena CO as well as AO have a strong impact on the resistivity. This results in three distinct anomalies to be identified upon cooling: (i) a broad minimum at elevated temperatures T_ρ of around 250 K, which is associated with a gradual charge localization, (ii) a sharp increase of $\rho(T)$ around $T_{CO} = 100$ K or so, which is related to ordering of the electronic charge, and (iii) a kink in resistivity due to the AO in the case of tetrahedral symmetry. Details are summarized in Table II and are discussed in the following.

(i) Localization: Cooling down from room temperature, the a axis resistivity slightly decreases and passes through a broad minimum between 200 and 300 K for all compounds except $(TMTTF)_2ReO_4$, which exhibits a negative slope $d\rho/dT < 0$ already at ambient temperature. The minimum in resistivity is an indication of localization effects, which do not result in a sharp phase transition but in a gradual freeze-out of the metallic conductivity. However, $\rho_{b'}$ and ρ_{c^*} exhibit an insulating behavior in the whole investigated temperature range, implying that, even at elevated temperatures, there is no coherent transport present in the perpendicular directions.

(ii) CO: In the temperature range between 157 and 67 K, a transition to a $4k_F$ CO state is observed in most $(TMTTF)_2X$ salts, such as $X = PF_6$, AsF_6, SbF_6, ReO_4, and BF_4. The effect can barely be detected in $(TMTTF)_2PF_6$, a distinct increase in the slope of the resistivity is seen in the salts with $X = AsF_6$, ReO_4, and BF_4, and an obvious kink in $\rho(T)$ characterizes the data of $(TMTTF)_2SbF_6$ at T_{CO}. The transition temperatures summarized in Table II are in good agreement with published data.[11–15] Surprisingly, not only the ordering phenomena are pronounced for transport along the a direction, but also the $\rho_{b'}(T)$ and $\rho_{c*}(T)$ are strongly effected as well, indicating the three-dimensional nature of the CO.

TABLE II. Transition temperatures for charge localization T_ρ, CO T_{CO}, and AO T_{AO} of various Fabre salts $(TMTTF)_2X$. T_{SP} indicates the spin-Peierls transition temperature.

	$(TMTTF)_2X$			
X	T_ρ (K)	T_{CO} (K)	T_{AO} (K)	T_{SP} (K)
PF_6	250	67		19
AsF_6	250	102		19
SbF_6	240	157		
BF_4	240	84	41.5	
ClO_4	260		73.4	
ReO_4		230	157	

(iii) AO: Subsequently, the compounds with tetrahedral anions undergo an AO transition at temperatures $T_{AO} < T_{CO}$, and the formed anion superstructure for all three investigated compounds is $q = (1/2, 1/2, 1/2)$, resulting in a $2k_F$ modulation along the stacking direction. In Fig. 3, the resistance at the transition is depicted for the b' direction, as an example. Upon cooling, a sharp downstep in resistivity is observed for $X = BF_4$ and ClO_4; it is more abrupt in the latter compound. In contrast to these two specimens, in $(TMTTF)_2ReO_4$, the AO appears as a steep step up at T_{AO}, followed by an increase in resistivity for $T < T_{AO}$.

Since this structural change of the AO marks a first-order phase transition, a hysteretic behavior is expected. Our data show only slight hysteresis observed when the warm-up curve is compared to the cooling curve. In the case of BF_4 as an anion, we find $\delta T \approx 0.5$ K, while for $(TMTTF)_2ClO_4$, the hysteresis is as big as 1.5 K. For $(TMTTF)_2ReO_4$, no hysteretic behavior is observable, as demonstrated in Fig. 3.

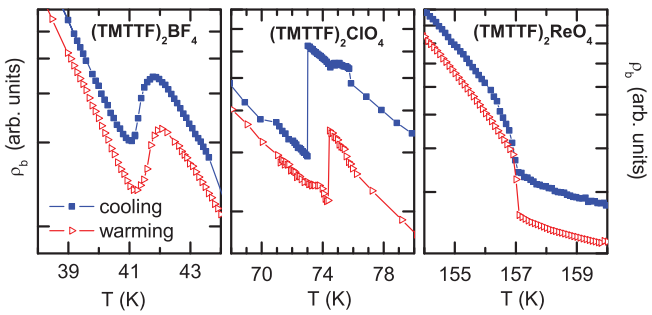

FIG. 3. (Color online) Enlarged view of the temperature-dependent resistivity $\rho_{b'}(T)$ of $(TMTTF)_2X$ for $X = BF_4$, ClO_4, and ReO_4 in the range of the AO. The slight shift of the transition temperature T_{AO} upon cooling down and warming up evidences the first-order phase transition. For clarity reasons, the curves are vertically displaced with respect to each other.

The observations at the AO are basically identical for all three directions; this implies a strong coupling between the anions in all directions leading to three-dimensional order. It is in full accord with structural investigations by diffusive x-ray scattering.[12–14]

IV. ANALYSIS

A. Transport mechanisms

In order to analyze the temperature-dependent resistivity quantitatively and to compare it with theoretical predictions, it is crucial to take the thermal expansion into account that is known to be considerable for these organic charge-transfer salts. From our data, $\rho^{(p)}(T)$ taken at ambient pressure p, resistivity at constant volume $\rho^{(V)}(T)$ is obtained via

$$\rho^{(V)}(T) = \frac{\rho^{(p)}(T)}{1 + 0.1\ \text{kbar}^{-1}\, p(T)}, \tag{1}$$

where $p(T)$ is the pressure required to compensate the thermal expansion with respect to the low-temperature unit cell at $T = 16$ K.[5] According to Mihály *et al.*[16] and Rose *et al.*,[17] the resistivity decreases by about 10% per kilobar for all temperatures above 50 K that are relevant for the present paper. We assume a similar behavior for all compounds and directions.

As mentioned above, along the b' and c^* directions and for $T < 200$ K also along the a axis, the resistivity always increases with decreasing temperature. Different temperature-dependent transport mechanisms can account for such a semiconducting behavior. For band transport, the resistivity follows the Arrhenius law,

$$\rho_{\text{dc}}^{(V)}(T) = \rho_0 \exp\left(\frac{\Delta}{T}\right). \tag{2}$$

If the energy gap Δ is temperature independent, the logarithm of the resistivity should be linear in $1/T$. The left panels of Figs. 4 and 5 show that this is only the case for transport along the c^* axis at elevated temperatures above the ordering transitions. Along the stacking direction, we cannot identify a sufficiently large range of simple thermally activated transport according to Eq. (2).

An alternative transport process is phonon-activated hopping between localized states, which, in disordered materials, is commonly described by the variable-range-hopping model proposed by Mott:[18]

$$\rho_{\text{dc}} \propto \exp\left[\left(\frac{T_0}{T}\right)^{1/\gamma}\right], \tag{3}$$

where $\gamma = d + 1$ is related to dimension d of the system. The right panels of Figs. 4 and 5 indicate that the transport in all compounds is governed by three-dimensional hopping below approximately $T = 60$ K. As expected from the very similar overall behavior, the quasi-one-dimensional nature of the material does not influence this incoherent transport process: $d = 3$; the anisotropy only enters the prefactor but not the power law. The extracted values for T_0 are listed in Table III. It has been predicted[19] that interaction between localized electronic states creates a so-called Coulomb gap in the density of states near the Fermi level that reduces the exponent $1/\gamma$ in Eq. (3) from 1/4 to 1/2. This effect seems not to have a strong influence in the present case.

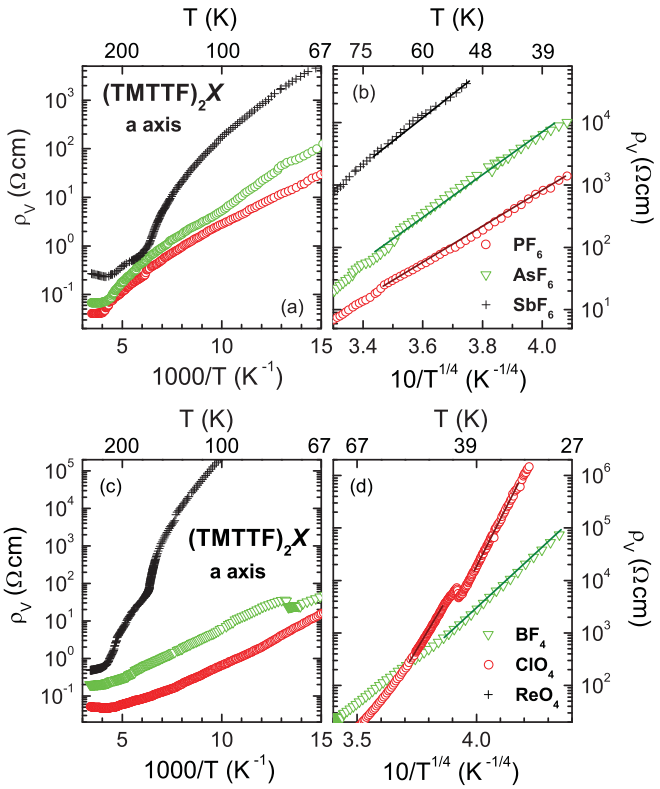

FIG. 4. (Color online) Parallel-stack dc resistivity $\rho_a^{(V)}(T)$ of various Fabre salts. The constant-pressure data are corrected according to Eq. (1) to account for the thermal expansion. The upper panels (a) and (b) summarize the results for the octahedral anions $(TMTTF)_2PF_6$, $(TMTTF)_2AsF_6$, and $(TMTTF)_2SbF_6$; while in the lower panels (c) and (d), the data for the tetrahedral anions $(TMTTF)_2BF_4$, $(TMTTF)_2ClO_4$, and $(TMTTF)_2ReO_4$ are shown. On the left side (a) and (c), the high-temperature data are plotted as a function of T^{-1}, and on the right side (b) and (d), the low-temperature regime is presented as a function of $T^{-1/4}$.

B. Temperature evolution of the energy gap

Along the a axis, neither of the models can satisfactorily fit the data at higher temperatures. If the current is applied

TABLE III. Extracted parameters T_0 of Mott's law [Eq. (3)] in the case of three dimensions ($\gamma = 4$) for the various compounds and different crystal axes; all values are given in units of 10^6 K.

	$(TMTTF)_2X$		
	T_0 (10^6 K)		
X	a direction	b' direction	c^* direction
BF_4	1249	1649	2012
ClO_4	82	59	279
ReO_4	795	633	909
PF_6	20	68	41
AsF_6	28	23	37
SbF_6	31	38	27

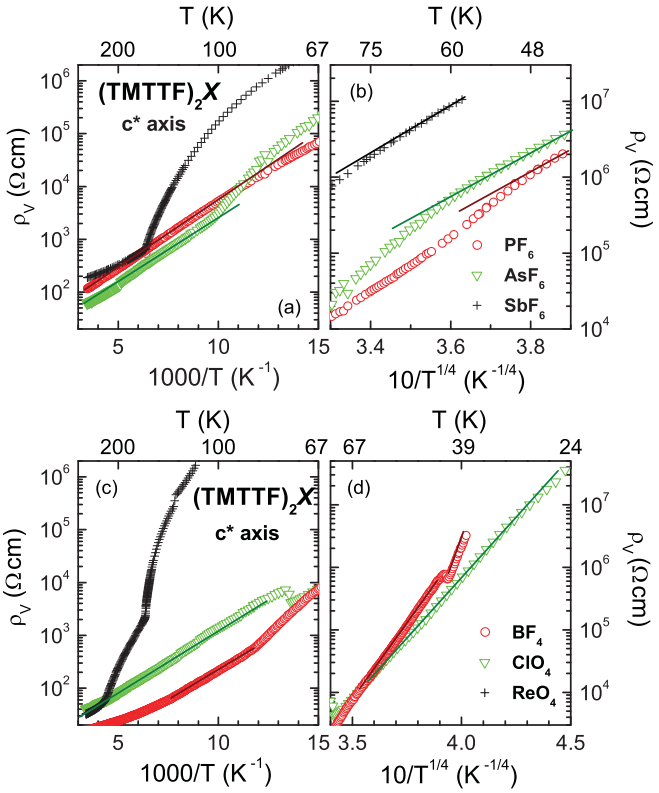

FIG. 5. (Color online) Direct-current resistivity $\rho_c^{(V)}(T)$ along the c^* direction of $(TMTTF)_2AsF_6$, $(TMTTF)_2PF_6$, and $(TMTTF)_2SbF_6$ as a function of (a) T^{-1} and (b) $T^{-1/4}$. In the lower panels (c) and (d), the same representation for the results of $(TMTTF)_2BF_4$, $(TMTTF)_2ClO_4$, and $(TMTTF)_2ReO_4$. The constant-pressure data are corrected according to Eq. (1) to account for the thermal expansion.

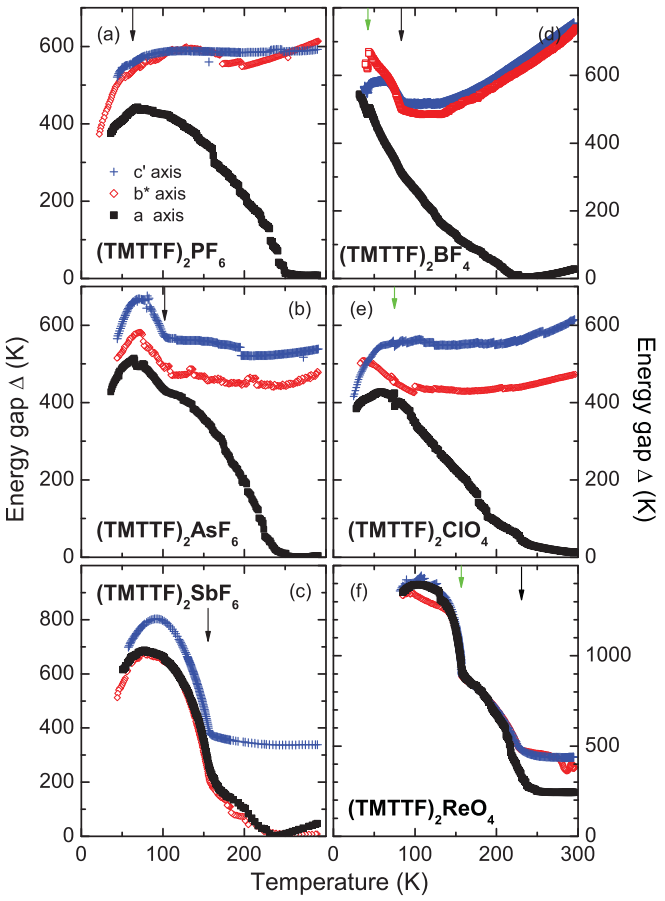

FIG. 6. (Color online) Energy gaps of $(TMTTF)_2X$ as a function of temperature along the a, b', and c^* axes. The activation energy was determined from the constant-volume data of the resistivity according to Eq. (4), choosing an appropriate value of $\rho(T)$. The small green arrows indicate T_{AO}, the larger black arrows denote the CO temperature T_{CO}.

parallel to the c^* axis, on the other hand, both models fail in the regions below the CO transitions and also the AO transition in $(TMTTF)_2ReO_4$. Hence, we abandon the assumption of a constant activation energy Δ in Eq. (2). Since the CO transition is a second-order phase transition, we expect a mean-field temperature dependence of the energy gap. In Fig. 6, the temperature-dependent energy gap,

$$\Delta(T) = \ln\left(\frac{\rho^{(V)}(T)}{\rho_0}\right) T \qquad (4)$$

is plotted as a function of T for all compounds and directions investigated, assuming constant ρ_0 as listed in Table IV. It immediately becomes obvious that the observed behavior is more complex and requires a detailed discussion. The following considerations are based on the idea that only temperature-dependent changes of the gap and no other effects are responsible for $\rho(T)$.

Basically, for all curves plotted in Fig. 6, the energy gap reaches a maximum well below T_{CO} and starts to decrease for even lower temperatures. In general, this is an indication of two processes with different temperature dependences. From the fit to Eq. (3) presented in panels (b) and (d) of Figs. 4 and 5, we know that, in this low-temperature range, the hopping of charge carriers between localized states starts to contribute to the electronic transport. This second contribution taints the analysis of $\rho(T)$ in terms of the Arrhenius law and cannot be adjusted for by a temperature-dependent gap. Therefore, we determine the hopping conductivity in the

TABLE IV. Prefactor of resistivity ρ_0 used in the determination of the temperature-dependent energy gap according to Eq. (4). We assumed the gap to vanish at T_ρ for transport along the a direction. For the b' and c^* directions, a constant gap Δ_0 was assumed for the temperature range above T_ρ but close to the first-ordering transition [usually the CO transition, except in $(TMTTF)_2ClO_4$]. Here, ρ_0 was extracted by a fit to the corresponding Arrhenius plot.

$(TMTTF)_2X$			
	ρ_0 (Ω cm)		
X	a direction	b' direction	c^* direction
BF_4	0.047	0.38	1.22
ClO_4	0.19	0.25	5.0
ReO_4	0.21	0.95	7.3
PF_6	0.068	0.33	15
AsF_6	0.068	0.55	9.5
SbF_6	0.229	0.9	58

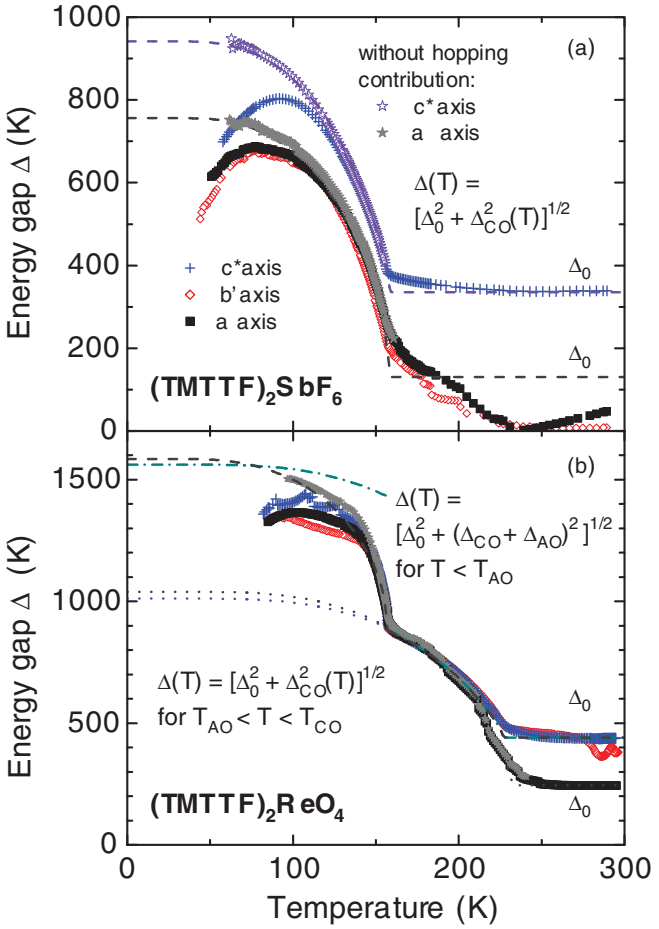

FIG. 7. (Color online) (a) Energy gaps of $(TMTTF)_2SbF_6$ as a function of temperature along the a, b', and c^* axes. The contribution by the hopping conduction to the transport $[\rho_{c^*}^{\mathrm{hop}}(T) = (4.31 \times 10^{-5}\ \Omega\,\mathrm{cm})\exp(72.45\ \mathrm{K}/T^{1/4})$, $\rho_a^{\mathrm{hop}}(T) = (39.8 \times 10^{-3}\ \Omega\,\mathrm{cm})\exp(74.5\ \mathrm{K}/T^{1/4})]$ was subtracted, and the remaining curve was fitted by Eq. (5) (dashed line), shown here, exemplary only for two crystal directions. (b) To eliminate the hopping conduction for $(TMTTF)_2ReO_4$, the dotted curves are obtained by a fit with Eq. (5). Below the AO transition, an additional gap opens, and the complete behavior follows Eq. (6) (gray dashed line). The fit for a temperature-independent gap Δ_{AO} is indicated by the dashed-dotted curve (cyan). Activation energies obtained from the fits are listed in Table V for the limit $T \to 0$.

low-temperature limit and subtract this contribution from the total conductivity in order to arrive at a purely activated behavior. As seen in Fig. 7 for the examples of $(TMTTF)_2SbF_6$ and $(TMTTF)_2ReO_4$, now the energy gap monotonically increases with decreasing temperature and finally levels off.

Obviously, two regions can now be distinguished in the curves of Fig. 7. At high temperatures, the energy gap is more or less temperature independent with a value Δ_0 of a few hundred Kelvin. The reason for this high-temperature energy gap is still under discussion, but commonly is related to the bond dimerization, resulting in an unequal distribution of the charge between the molecules. Cooling through T_{CO}, the electronic charge on the molecular sites becomes disproportionate due to CO. The CO gap exhibits a BCS-like increase with lowering the temperature and amounts up to approximately 1000 K. Qualitatively, the same behavior (at $T < T_{\mathrm{CO}}$) is observed for all specimens and directions. The total energy gap, consisting of these two contributions, is well described by

$$\Delta(T) = \sqrt{\Delta_0^2 + \Delta_{\mathrm{CO}}^2(T)}, \tag{5}$$

following the idea that these two effects cause a spatial modulation of the potential, however, displaced by a quarter of a wavelength.[7,8] Only in some cases does the energy gap seem to be slightly temperature dependent above T_{CO}, which prevents an unambiguous decomposition and satisfactory description.

In the case of tetrahedral anions, a second transition occurs at T_{AO}, causing a further energy gap Δ_{AO} to open in most of the $(TMTTF)_2X$ compounds. As demonstrated in Fig. 7(b) for the example of $(TMTTF)_2ReO_4$, it can be described best by an additional temperature-dependent (BCS-like) energy gap. This result is surprising considering the nature of the AO transition. Usually, structural transitions are of first order, and in $(TMTTF)_2ReO_4$, the AO is attended by the doubling of the unit cell along the a direction. Hence, intuitively, the expectations are a temperature-independent gap Δ_{AO}, but this does not allow for a satisfactory description [dashed-dotted line in Fig. 7(b)] of the results. The temperature dependence of Δ_{AO} infers that the gap is not just caused directly by the anion potential, but the main contribution comes via changes in the TMTTF stacks triggered by the AO, e.g., modifications of the on- and off-site potentials. These changes result in different charge concentrations on and between the organic molecules and alter the backscattering potentials felt by the charged particles participating in transport. If one takes this mechanism into account, the spatial modulation of the CO effect and the resulting changes caused by the AO are in phase. The total energy gap is then described by

$$\Delta(T) = \sqrt{\Delta_0^2 + [\Delta_{\mathrm{CO}}(T) + \Delta_{\mathrm{AO}}(T)]^2}. \tag{6}$$

Let us now consider the various compounds in more detail to point out their peculiarities.

(i) $(TMTTF)_2X$ ($X = PF_6, AsF_6, SbF_6$): The CO transition in $(TMTTF)_2PF_6$ at $T_{\mathrm{CO}} = 67$ K only leads to a small increase of the energy gap along all three directions. It can be barely seen in Fig. 6(a) because, at that temperature, the hopping already dominates the transport behavior, and the transition seems to be smeared out. For $(TMTTF)_2AsF_6$, a mean-field-like increase in the energy gap of about 110 K is seen at $T_{\mathrm{CO}} = 103$ K along all three directions. Below 75 K, hopping transport dominates. In $(TMTTF)_2SbF_6$, the effects at the CO transition ($T_{\mathrm{CO}} = 157$ K) are most pronounced. Along all three axes, the energy gap increases by several hundred Kelvin. The temperature dependence has a BCS shape. As demonstrated in Fig. 7, the high-temperature gap and the CO gap add in quadrature [Eq. (5)]. If the contribution of the hopping transport to the conductivity is subtracted, the mean-field-like temperature dependence of the gap can be extracted to lowest temperatures with $\Delta_{\mathrm{CO}} \approx 800$ K. No indications of a first-order nature for the transition are found.

(ii) $(TMTTF)_2ClO_4$: No $2k_{\mathrm{F}}$ CO has been observed in this compound. At the AO transition ($T_{\mathrm{AO}} = 73$ K) of $(TMTTF)_2ClO_4$, the resistivity shows a sudden decrease (Fig. 3). However, from Fig. 6(e), we see that the slope in

the Arrhenius plot is unaffected by the jump, giving evidence that Δ is constant across the transition. Therefore, we attribute the abrupt change in the resistivity to the prefactor ρ_0 in Eq. (2). From Fig. 2, it becomes obvious that, at T_{AO}, ρ_0 decreases by the same factor of 2.5 for all three directions.

(iii) $(TMTTF)_2BF_4$: In the case of $(TMTTF)_2BF_4$, the jump in $\rho(T)$ at $T_{AO} = 42$ K is not so abrupt as in the ClO_4 counterpart. The effect is strongest along the b' axis and weakest along the c^* axis. A close inspection of the Arrhenius plot reveals a weak increase in the slope $d\rho/dT$ for $T < T_{AO}$. At these low temperatures, however, substantial contributions from hopping transport might be present and might obscure a precise analysis. Nevertheless, we estimate that ρ_0 decreases by about the same ratio as in $(TMTTF)_2ClO_4$, while the energy gap $\Delta(T)$ increases slightly as the temperature passes through the AO transition upon cooling. At $T_{CO} = 84$ K, the energy gap increases in a mean-field manner due to the opening of a CO gap. The rise is moderate and is best seen along the b' and c^* axes. The effect is diluted by the hopping transport, which becomes dominant in this temperature range.

(iv) $(TMTTF)_2ReO_4$: In this compound, strong contributions to the gap are observed by the CO and by the AO. When cooling through the CO transition ($T_{CO} = 223$ K), the energy gap $\Delta(T)$ increases by several hundred Kelvin, in a similar fashion for all three axes. As demonstrated in Fig. 7(b), the temperature dependence of the gap resembles a BCS-like shape. Following Eq. (5), the total energy gap is a result of the contribution due to temperature-independent charge localization and the CO adding up in quadrature. As mentioned above, $(TMTTF)_2ReO_4$ exhibits a completely different behavior in the conductivity at T_{AO}, where the increase in $\rho(T)$ can be described by Eq. (6). The enhancement of the gap is not abrupt but is stronger than expected for a second-order transition. In the low-temperature limit, the extra contribution to the activation energy in the AO state is very similar for all three directions. One reason for the particular behavior of $(TMTTF)_2ReO_4$—and similar $(TMTTF)_2FSO_3$—is the large size of the anions, which modifies the array of the TMTTF molecules.[20]

In Table V, we list the activation energies Δ obtained from our analysis of $\rho(T)$ for all the compounds investigated; in addition, we give the individual contributions of the charge localization Δ_0, the CO Δ_{CO}, and the AO Δ_{AO}. Only $(TMTTF)_2AsF_6$ has previously been analyzed along all three directions;[10] the published activation energies agree very well with the present findings. Nad and Monceau[15] measured the dielectric response in the stacking direction and were able to extract activation energies for several of the TMTTF compounds; except for the AsF_6 and PF_6 salts, their values are in good accord with our results.

TABLE V. Summary of the activation energies obtained from Fig. 6 in the three directions of the various $(TMTTF)_2X$ salts. In the localization regime $T_\rho > T > T_{CO}$, an energy gap Δ_0 is dominant. The CO regime $T_{CO} > T > T_{AO}$ is governed by Δ_{CO}; below the AO-transition temperature $T_{AO} > T$, the energy gap Δ_{AO} gives an additional contribution in the case of $(TMTTF)_2ReO_4$. Δ is the total energy gap in the limit $T \to 0$ K. $\vartheta(T)$ considers some additional temperature dependence; uncertain cases are indicated by parentheses; sometimes only very rough estimates are possible.

$(TMTTF)_2X$				
Direction	Δ_0 (K)	Δ_{CO} (K)	Δ_{AO} (K)	Δ (K)
		$X = PF_6$		
a	$440 \pm \vartheta(T)$	Small		440 ± 20
b'	590 ± 30	Small		590 ± 30
c^*	590 ± 10	Small		590 ± 10
		$X = AsF_6$		
a	$420 \pm \vartheta(T)$	310		520
b'	460 ± 20	370		590
c^*	540 ± 20	410		680
		$X = SbF_6$		
a	$130 \pm \vartheta(T)$	745 ± 20		760 ± 30
b'	$130 \pm \vartheta(T)$	745 ± 20		760 ± 30
c^*	340 ± 20	880 ± 20		940 ± 30
		$X = BF_4$		
a	$320 \pm \vartheta(T)$	(Medium)	Small	(600)
b'	$[500 \pm \vartheta(T)]$	Medium	Small	(600)
c^*	$520 \pm \vartheta(T)$	310	Small	600
		$X = ClO_4$		
a	$430 \pm \vartheta(T)$		0	430 ± 50
b'	(440 ± 60)		0	(440 ± 60)
c^*	560 ± 50		0	560 ± 50
		$X = ReO_4$		
a	245 ± 50	1010 ± 50	530 ± 20	1560 ± 60
b'	440 ± 70	910 ± 50	590 ± 20	1560 ± 80
c^*	440 ± 50	910 ± 50	590 ± 20	1560 ± 60

C. Anisotropic transport

If the temperature is low enough, no coherent transport exists in $(TMTTF)_2X$ compounds along any of the three axes; instead, hopping transport is observed in the a, b', and c^* directions.[21] At high temperatures, the situation is not that clear and well resolved. Along the b' axis, a more or less temperature-independent energy gap is found in all compounds but $(TMTTF)_2SbF_6$ and $(TMTTF)_2ReO_4$. The values are in the same range or up to 100 K smaller than in the c^* direction.

(i) a axis: The a axis resistivity goes through a minimum in most compounds, which corresponds to a zero energy gap, as seen in Fig. 6. Then, with decreasing T, the gap increases up to 400 K. There are some abrupt changes in the temperature-dependent gap due to the ordering transitions.

(ii) c^* axis: For $T > 100$ K and above any ordering temperature, the charge transport along the c^* direction is thermally activated with a corresponding energy of approximately 540 ± 40 K. Following Georges *et al.*,[22] we conclude that the c^*-axis dc data evidence thermally activated behavior, with an activation energy equal to the charge gap Δ_0, which is very similar for all TMTTF salts. Somewhat smaller values are observed in the compounds with higher-ordering temperatures, such as $(TMTTF)_2ReO_4$ ($\Delta_0 = 440$ K) and $(TMTTF)_2SbF_6$ ($\Delta_0 = 340$ K). In these compounds, the results might be influenced by the high transition temperatures and fluctuations.

At low temperatures ($T < 70$ K and temperatures not too close to the CO transition), the resistivity exhibits the Mott

$T^{1/4}$ law for hopping transport [Eq. (3)]. As demonstrated in Fig. 7, the low-T conductivity can be described very well by the sum of an Arrhenius and a $T^{1/4}$ behavior. These are two completely separate concepts of electronic transport, which seem to exclude each other. On one hand, our experimental findings of the Arrhenius law suggest band transport above 100 K, while hopping transport is dominant well below that temperature. On the other hand, it is known that, in the TMTTF salts, the molecular chains are well separated along the c axis and that the hopping integral t_c is rather small (less than 1 meV), which does not allow for any considerable overlap of the molecular orbitals.

(iii) b' axis: Along the b' axis, the same arguments apply as along the c^* direction, however, the hopping integrals (orbital overlap) and, thus, the absolute values of conductivity are considerably larger. We expect the energy gaps derived from the Arrhenius law being temperature independent and isotropic, because it always originates from the effective Coulomb repulsion on the chains. Hence, the resulting resistivity exhibits the same temperature dependence in all directions, assuming that the hopping integrals are temperature independent and that no other contributions to the charge transport are present. Our results suggest that this condition is fulfilled best along the c^* axis.

V. DISCUSSION

According to band-structure calculations, the $(TMTTF)_2X$ compounds develop bands along the a direction, which are 1/4 filled by chemistry. Due to a slight dimerization of the chains, the conduction band is split and effectively is half filled. Thus, one would expect coherent metallic transport along the chains, and this agrees with the $\rho_a(T)$ that we observe at elevated temperatures. On-site Coulomb repulsion U splits the conduction band in upper and lower Hubbard bands by a Mott gap Δ_0. Correspondingly, below $T_\rho \approx 250$ K, the transport becomes thermally activated according to Eq. (2). As CO develops for $T < T_{CO}$, the gap enlarges upon cooling. In the case of AO, its size increases even more in most compounds.

The small transfer integrals ($t_b \approx 10$ meV and $t_c \approx 1$ meV) prevent coherent charge transport in the perpendicular directions, and one would expect diffusive motion only. In fact, insulating behavior is observed in the perpendicular directions at all temperatures. However, variable-range hopping causes a very distinct temperature dependence, given in Eq. (3), for instance, which could only be identified at very low temperatures (right panels of Fig. 5). The intriguing question is why, most of the time, the perpendicular transport basically follows the behavior parallel to the chains at reduced temperatures, except for some factor. This immediately implies that diffusive transport does not influence the temperature dependence of $\rho_{b'}$ and ρ_{c^*} and that $t_\perp$ mainly contributes to the prefactor. Thermally activated transport is the dominant mechanism perpendicular to the stacks. Even when tunneling between the chains, the charge carriers have to overcome the energy gaps that open in the conduction band due to Coulomb repulsion, CO, and AO. The behavior of $\rho_{b'}(T)$ and $\rho_{c^*}(T)$ reflects the changes in the one-dimensional band. Only for temperatures clearly above T_{CO}, the temperature dependences of $\rho_{b'}$ and ρ_{c^*} might resemble the purely perpendicular transport not influenced by properties of the a direction.

TABLE VI. Structural data for the different $(TMTTF)_2X$ compounds assembled from Refs. 34–38. The values for the dimerization in $(TMTTF)_2PF_6$ and $(TMTTF)_2SbF_6$ are from Ref. 39.

	$(TMTTF)_2X$			
X	a (Å)	b (Å)	c (Å)	$\Delta d_a/\langle d_a\rangle$
BF_4	7.112	7.468	12.946	1.13×10^{-2}[a]
ClO_4	7.155	7.515	12.992	1.89×10^{-2}[a]
ReO_4	7.158	7.613	13.231	2.10×10^{-2}[a]
PF_6	7.157	7.580	13.213	2.63×10^{-2}
AsF_6	7.178	7.610	13.317	2.97×10^{-2}[a]
SbF_6	7.180	7.654	13.507	3.24×10^{-2}
	α (°)	β (°)	γ (°)	V (Å^3)
BF_4	85.56	85.95	71.20	648.2
ClO_4	84.41	85.27	71.53	648.8
ReO_4	82.68	84.57	71.79	678.2
PF_6	82.64	84.72	72.41	676.6
AsF_6	82.03	84.25	72.89	697.7
SbF_6	81.24	83.42	74.00	702.9

[a]Data extracted from the associated CIF file.

Within the group of symmetric and nonsymmetric anions, there are trivial relations of the absolute values $\rho(300\ \mathrm{K})$ in the three directions to the corresponding lattice parameter summarized in Table VI and Fig. 11. The absolute value of $\rho(300\ \mathrm{K})$ depends on the orbital overlap defined by the distance and position of the organic molecules with respect to each other. Along the a axis, the transfer integrals determine the bandwidth, along the two other crystal directions, they affect the tunneling probability. This description does not include any correlation effects that might have an impact even on the room-temperature resistivity, e.g., fluctuations found by Coulomb repulsion or rotating anions causing localization effects. Transfer integrals and correlation effects can be changed by chemical or physical pressure. A detailed investigation of the pressure dependence for these charge localization and ordering effects will be given elsewhere (Ref. 17).

A. Anisotropic transport mechanism

There have been multiple attempts to theoretically describe the transport in anisotropic conductors. Ishiguro *et al.*[23] considered one-dimensional metallic chains connected by diffusive conduction and suggested that the ratio of the conductivity parallel and perpendicular to the stacks is

$$\frac{\sigma_\parallel}{\sigma_\perp} = \frac{\hbar^2 v_F^2}{2b^2 t_\perp^2}, \tag{7}$$

where v_F is the Fermi velocity along the stacks and b and $t_\perp$ are the distance and transfer integrals of the adjacent stacks. This approach is applicable only when transport is coherent along the chains ($\sigma_\parallel$) and incoherent in the perpendicular direction

($\sigma_\perp$). Using tight-binding approximation for a quarter-filled band, resulting in $\hbar v_F = \sqrt{2} t_\parallel a_s$, with a_s equal to the distance of the molecules (unit-cell length $a = 2a_s$), one ends up with[4,24]

$$\frac{\sigma_\parallel}{\sigma_\perp} = \left(\frac{a_s}{b}\right)^2 \left(\frac{t_\parallel}{t_\perp}\right)^2. \quad (8)$$

With regard to $(TMTTF)_2X$, this relation is only valid within the temperature range $T > T_\rho$, and calculations for $(TMTTF)_2PF_6$ yield 1:16:860 for the anisotropy, reproducing our experimental data (cf. Table I) within a factor of 3.

Equation (7) can be extended to the gapped system when replacing v_F by the thermal velocity $v_T = \sqrt{k_B T/m^*}$,[23]

$$\frac{\sigma_\parallel}{\sigma_\perp} = \frac{\hbar^2 k_B T}{2m^* b^2 t_\perp^2}. \quad (9)$$

This equation is only valid for very low carrier concentration, when phase-space restrictions are not important anymore and the Fermi distribution can be replaced by the Boltzmann distribution. For $(TMTTF)_2X$ and $T < T_\rho$, the overall temperature dependence of the measured anisotropy is in agreement with Eq. (9) for the gapped system.

These predictions assume perfect crystals and do not take defects and imperfections of real samples into account. Under extreme conditions, e.g., when the gap in the conduction band is very large, contributions from variable-range hopping between localized states may exceed band transport. This is reflected in our measurements, when, for very low temperatures, $\rho(T)$ deviates from Arrhenius law, changing to the temperature dependance of hopping transport.

B. Luttinger liquid

All investigated $(TMTTF)_2X$ salts are one-dimensional conductors and are located in the Luttinger-liquid regime for high temperatures. When T is lowered, electronic correlations become relevant and open up a gap Δ_0 in the electronic density of states, i.e., drive the system into a Mott insulating state (cf. phase diagram Fig. 8). Due to the high localization temperature T_ρ of about 250 K, it is difficult to extract Luttinger exponents from our measurements. Transport studies at elevated temperatures are highly desirable, however, the crystals decompose at approximately 400 K.

In the Bechgaard salts $(TMTSF)_2X$, a dimensional crossover is reported upon cooling or application of pressure,[25–28] for example, seen in the development of a Drude-type conductivity and plasma edge in the optical properties of the b direction. In the case of the sulfur analogs, such as $(TMTTF)_2PF_6$, pressure has to well exceed 20 kbar.[28] This is in full agreement with the (about a factor of 4) different values for the transfer integrals t_b of the selenium and sulfur analogs, for instance, $(TMTSF)_2PF_6$: $t_b \approx 56$ meV and $(TMTTF)_2PF_6$: $t_b \approx 13$ meV.[29,30]

C. Charge localization

The metal-like conduction at elevated temperatures vanishes around 250 K basically for all $(TMTTF)_2X$ compounds, and charge localization sets in due to the opening of a Mott gap. In the range above the ordering temperature, transport

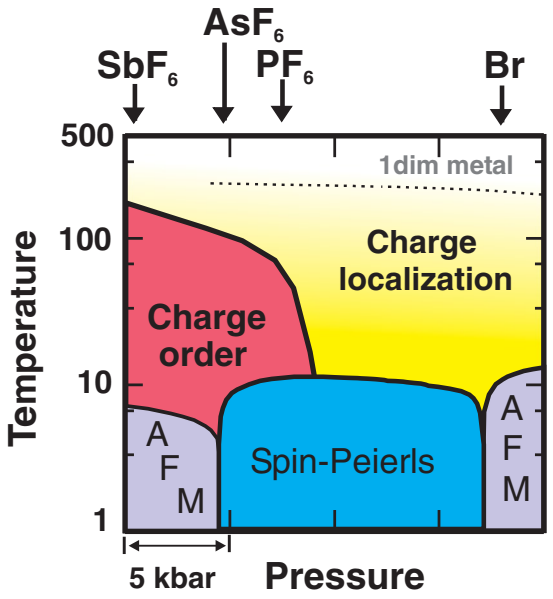

FIG. 8. (Color online) The phase diagram of $(TMTTF)_2X$ shows the different phases (AFM, spin-Peierls, CO, charge localization, and one-dimensional metal) as a function of pressure. While some of the boundaries are clear phase transitions, the ones indicated by dashed lines are better characterized as a crossover. The position in the phase diagram can be tuned by chemical pressure or external pressure with the approximate scale given. For the different compounds with octahedral and spherical anions, the ambient-pressure position in the phase diagram is indicated by the arrows on the top axis.

is characterized by an average activation energy Δ_0 on the order of 500 $\pm$100 K for most compounds. With increasing anion size, the energy Δ_0 decreases; however, there seems to be no simple relation to the dimerization observed in these compounds (Tables V and VII). Williams *et al.*[31] pointed out a relation to the unit-cell volume and the S-S contacts, which both increase when going from $X = BF_4$ to ReO_4 and further to SbF_6 (Fig. 11). Regarding the theoretical description of Δ_0, different factors have to be taken into account. The nominal band filling of the $(TMTTF)_2X$ compounds is 1/4, but due to the structural dimerization of periodicity $4k_F$, a band gap opens up, moving the system toward half filling.[32] Due to umklapp scattering, the system develops the Mott gap Δ_0. Following Giamarchi,[33] the strength of the umklapp scattering is described for half- and quarter-filled systems by $g_{1/2} \propto U(D/E_F)$ and $g_{1/4} \propto U(U/E_F)^2$, respectively, where U stands for on-site Coulomb repulsion, E_F is the Fermi energy, and D denotes the dimerization gap. The strength of the dimerization D is difficult to estimate, since it is caused by bond or on-site dimerization or by the anion potential. Considering only bond dimerization along the a direction, the data for $\rho_a(T)$ show a linear relation within symmetric or nonsymmetric anions, plotted in Fig. 9 as a function of the relative dimerization $2(d_2 - d_1)/(d_2 + d_1)$.

It is interesting to note that, for the perpendicular transport ρ_{c^*}, the ambient-temperature values increase monotonously when going from $X = BF_4$ to SbF_6 despite the different symmetry (Fig. 9).

TABLE VII. The relative dimerization $\Delta t_s/\langle t_s\rangle$ is determined by structural studies of different Fabre salts. The room-temperature values are taken from Nogami *et al.*;[50] those in brackets are from Refs. 7,20,51. The values for the dimerization in $(TMTTF)_2PF_6$ and $(TMTTF)_2SbF_6$ are from Ref. 39; for the other compounds the data are extracted from the associated CIF file.

$(TMTTF)_2X$				
	$\Delta t_s/\langle t_s\rangle$		δ	
X	$T \approx 300$ K	Low T	NMR	IR
PF_6	0.41 (0.38)	0.20 (30 K)	0.12 (30 K)	0.06 (30 K)
AsF_6	0.46 (0.34)	0.19 (40 K)	0.13 (30 K)	0.13 (20 K)
SbF_6	0.39 (0.30)	0.17 (100 K)	0.25 (low)	
ClO_4	0.34 (0.33)			
ReO_4	0.45	0.30 (150 K)	0.17 (100 K)	

D. Charge-order

Except $(TMTTF)_2ClO_4$, all Fabre salts develop a CO phase below $T < T_{CO}$, as first observed in thermopower and resistivity measurements. Interestingly, there is no decrease or distinct anomaly in the magnetic susceptibility:[40] Unlike common semiconductors, the spin is not affected by charge activation. The CO phase was finally proven by nuclear magnetic resonance (NMR),[41,42] dielectric,[15,43,44] and optical measurements[45,46] and amounts to a few percent as listed in the right columns of Table VII.

The charge disproportionation results from an interplay of on-site and next-neighbor repulsion U and V, respectively. While this phenomenon is clear for quarter-filled compounds, it is still under discussion for systems close to half filling, which might be the case in $(TMTTF)_2X$ due to the structural dimerization of periodicity $4k_F$. It has been argued[20] that there is a strong competition between the dimeric Mott state and the CO state. According to Nogami *et al.*,[50] the relative dimerization $\Delta t_s/\langle t_s\rangle = 2(t_{s1} - t_{s2})/(t_{s1} + t_{s2})$ decreases strongly from its room-temperature value of 0.4–0.45 when the temperature is reduced and reaches approximately 0.25 at T_{CO}. Values of $\Delta t_s/\langle t_s\rangle$ larger than 0.25 prevent $4k_F$ site CO in $(TMTTF)_2X$. This can be interpreted, that compared to half-filled properties, quarter filling has to dominate in these systems in order to exhibit CO. In Table VII, the available values for dimerization and charge disproportionation are listed.

For a long time, the CO transition in $(TMTTF)_2X$ was considered of purely electronic origin and was called a structureless transition.[48] Since no additional spots could be found in x-ray scattering,[49,50] the possible structural changes had to be very small. Only recently, high-resolution thermal expansion measurements[52] revealed a pronounced anomaly in $(TMTTF)_2PF_6$ and $(TMTTF)_2AsF_6$ at the CO transition, that is much stronger pronounced along the c^* and b' axes than along the chains. These results support early suggestions of Pouget[53] and others[8] that CO is stabilized by structural modifications, in particular, by the anions.[54]

The fact that CO is linked to the anion arrangement becomes obvious from Fig. 10: A nearly linear correlation is discovered when the CO transition temperature T_{CO} is plotted versus the shortest distance between the sulfur atoms in the TMTTF molecule and the ligands of the anions, i.e., fluorine or oxygen. Note, the only compound that does not develop charge disproportionation, by far, holds the longest distance.[55] The important interaction between the organic cations and the counterions was recently detected by electron spin resonance (ESR) spectroscopy, which revealed an anomalous temperature behavior for the g factor, indicating the deformation of the molecular orbitals by the anion potential.[56]

By comparing the shape of the anions for the different compounds, it is obvious, especially, that the nonsymmetric anions are strongly distorted; this calls for a closer inspection of the anions themselves. A short contact between the ligand and the organic molecule is naturally correlated with a long bond between the ligand and the central atom of the anion.

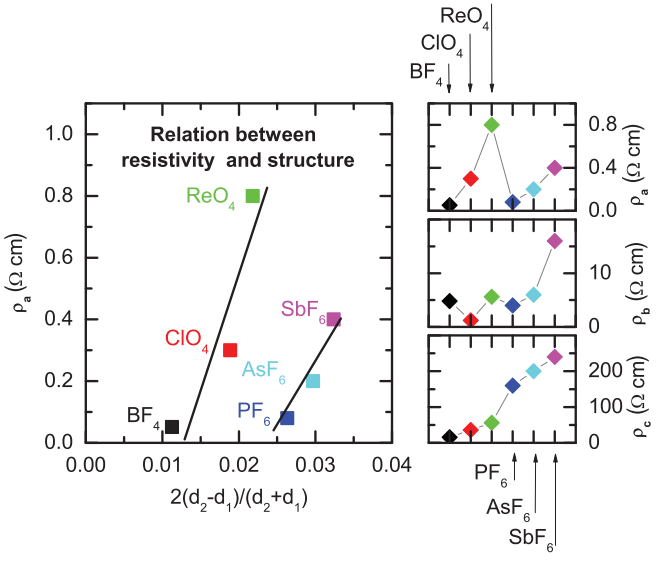

FIG. 9. (Color online) In the left panel, the dependence between the resistivity ρ_a and the structural dimerization along the a axis, both taken at room temperature, is plotted. The structural data are taken from Refs. 34–39. The right panels show the room-temperature resistivities ρ_a, $\rho_{b'}$, and ρ_{c^*} for all investigated compounds $(TMTTF)_2X$; from left to right, the volume of the unit cell increases, i.e., X = BF_4, ClO_4, ReO_4, PF_6, AsF_6, and SbF_6.

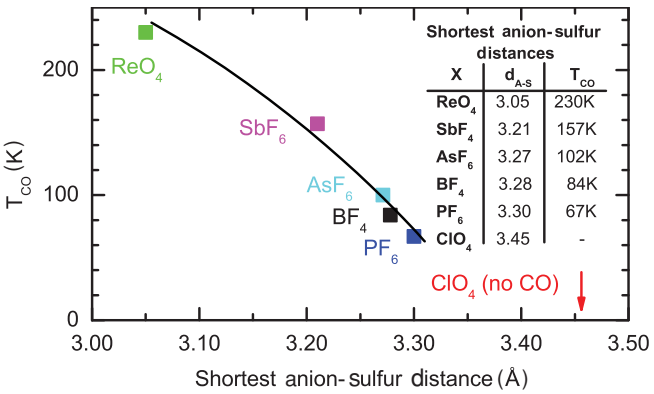

FIG. 10. (Color online) The CO transition temperature T_{CO} as a function of the shortest distance between the ligands of the anions (F or O) and sulfur atoms in TMTTF. For $(TMTTF)_2ClO_4$, the distance is much larger compared to the other compounds: It develops no CO. The structural data are taken from Refs. 34–39.

The bond length in the anions increases from ClO_4 over BF_4 to ReO_4. This is determined by the size of the central atom and the difference in electronegativity of the atoms constituting the anion.

Despite some ambiguity in extracting the slope in the Arrhenius plot,[57] the energy gaps deduced from our transport measurements (Table V) are in fair agreement with literature data. In general, the activation energy increases upon lowering the temperature from one regime to another. Below T_{CO}, the CO gap $\Delta_{CO}(T)$, following a BCS-like behavior, indicates a second-order phase transition. Since we start out from a charge-localized state, it adds to the present gap Δ_0 according to Eq. (5). The total activation energy is a consequence of bond and site contributions to the umklapp scattering, i.e., $\Delta = \Delta(U)$ and $U = \sqrt{U_b^2 + U_s^2}$.[8,58] Our assumption to add up the bond gap and the site gap according to Eq. (5) is not mandatory for pure electronic origin, but the good fit to our data justifies this assumption. It can be seen as an indication that the CO gap does not only have electronic origin, but also is stabilized by structural properties. It should be noted that significant differences exist for the various compounds, and the increase in the activation energy upon passing through the CO transition varies significantly. Thus, it is not possible to relate $\Delta_{CO}(T)$ to the value of the CO parameter δ used to characterize the charge disproportionation.

As depicted in Fig. 11, there seems to be some correlation between the various anions and the structural parameters. However, due to the different symmetry and distortion of the anions, a rigorous relation of unit-cell parameters with physical properties seems difficult. Further issues of relevance are the polarizability and how strong charge is located on the anion.

One important finding of our paper is the surprising similarity in the overall behavior in all three directions. This implies that the CO is coupled between the chains and influences the transport in a similar way. Brazovskii pointed out that, in the present case of a ferroelectric Mott-Hubbard insulator, ordered domains develop, separated by ferroelectric domain walls.[8] Further experimental and theoretical studies of the behavior in the perpendicular directions are highly desirable.

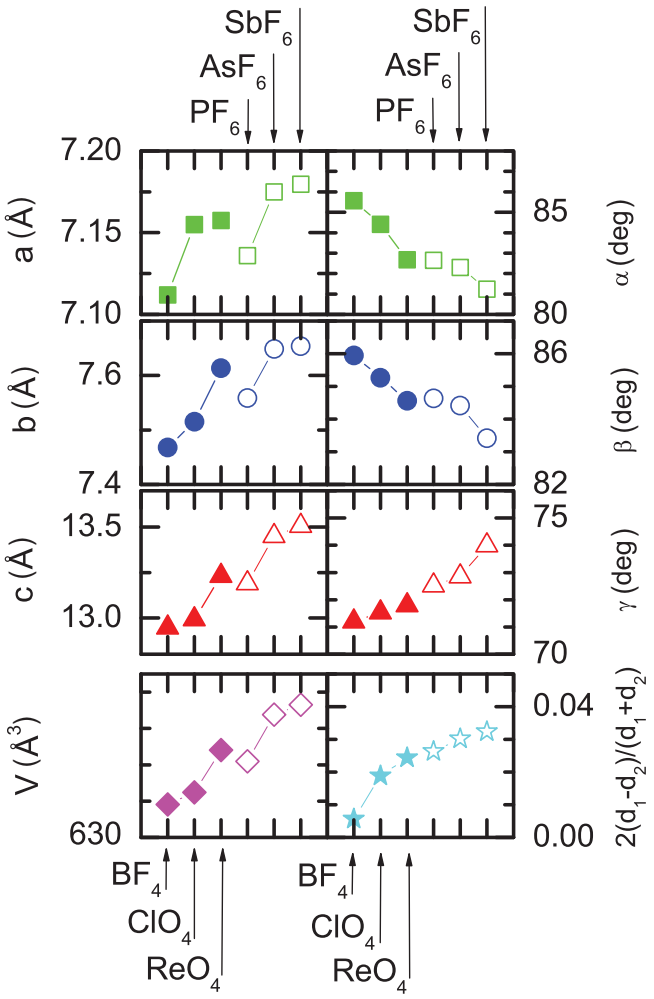

FIG. 11. (Color online) Unit-cell and dimerization parameters for the six investigated compounds of $(TMTTF)_2X$. The compounds are ordered from left to right by increasing unit-cell volume (X = BF_4, ClO_4, ReO_4, PF_6, AsF_6, and SbF_6). The structural data are taken from Refs. 34–39 and are tabulated in Table VI.

E. Anion-order

As demonstrated from Fig. 3, the AO anomaly in $(TMTTF)_2ClO_4$ is not associated with a noticeable change in the slope of resistivity $\rho(T)$, as already pointed out by Coulon *et al.*[11] Finding the identical activation energy on both sides of the phase transition implies that the dominant transport mechanism remains unchanged. In the case of $(TMTTF)_2BF_4$, a slight increase in the activation energy can be identified when passing T_{AO}. The maximum AO gap Δ_{AO} is found for $(TMTTF)_2ReO_4$, following a BCS-like temperature dependence.

For $X = BF_4$ and ClO_4, a steplike reduction in resistivity at T_{AO} is observed. It can be interpreted as a freezing out of scattering channels due to AO. The fact that the overall slope $\rho(T)$ does not change significantly above and below T_{AO} implies that the more or less temperature-independent scattering due to anion disorder—which adds to temperature-dependent factors according to Matthiessen's rule—just freezes out.

Taking these different characteristics of the AO in the investigated $(TMTTF)_2X$ compounds into account, the conclusion is obvious, that Δ_{AO} not only is generated by backscattering on the anion potential, but also is a consequence of the changes which the AO induces on the TMTTF molecules.[59] The value of Δ_{AO} depends, however, on the coupling between the anion and the TMTTF stack. The fact that, in $(TMTTF)_2SCN$, the metal-insulator transition occurs at T_{AO}, and the anion superstructure does not lead to a doubling of the unit cell along the a direction [$q = (0,1/2,1/2)$, Ref. 60] supports this idea. Recent ESR experiments corroborate this picture as well:[40] The AO in $(TMTTF)_2ReO_4$ leads to a very large singlet-triplet gap $\Delta_\sigma = 1100$ K because a o-O-O-o- charge pattern develops along the stacks below T_{AO}.

Coupling strength between the anions and the TMTTF stack seems not only to depend on the size of the anion, increasing from BF_4, ClO_4, to ReO_4, but also to have a more pronounced difference in the shortest distance from anions ligand to sulfur

(tabulated in the inset of Fig. 10) and the electronegativity of the atoms constituting the anions. Following this idea, coupling increases from ClO_4, BF_4 to ReO_4, whereas, the transition temperature depends on the anion size.

The step in $\rho(T)$ is the same in all three directions, implying that the ordering affects the transport in a similar way. We conclude that a three-dimensional order of the anions takes place at T_{AO}, i.e., there is strong coupling between the stacks, and the periodicity changes in all directions. These findings are in accord with previous and recent ESR experiments.[40,61]

VI. SUMMARY

The temperature-dependent dc resistivity of the quasi-one-dimensional organic salts $(TMTTF)_2X$ ($X = PF_6, AsF_6, SbF_6, BF_4, ClO_4, ReO_4$) was measured and was analyzed in all three directions. Most of the compounds exhibit a weak metallic behavior at elevated temperatures. Increasing charge localization leads to a resistivity minimum around $T_\rho = 250$ K, and the opening of an energy gap, which upon cooling, increases up to $\Delta_0 \approx 400$ K before CO sets in. Below T_{CO}, we can derive a gap $\Delta_{CO}(T)$ in the density of states that opens in a mean-field-like fashion. The effect is seen in all three crystal directions but is best resolved along the c^* axis. The resistivity increases in all compounds but to a different extent: In $(TMTTF)_2PF_6$, it is barely visible, the effect of CO is moderate in $(TMTTF)_2BF_4$ and AsF_6, and is very strong in $(TMTTF)_2SbF_6$ and $(TMTTF)_2ReO_4$. From our comparison of structural and transport data, we find relations of resistivity values to the anion size and the amount of dimerization; also, we can clearly identify the influence of the anions on the CO transition. AO in $(TMTTF)_2BF_4$ and $(TMTTF)_2ClO_4$ causes a steplike decrease in the resistivity below T_{AO} since disorder scattering is reduced. To the contrary, the energy gap of $(TMTTF)_2ReO_4$ increases strongly because of the much stronger influence of the anion on the organic stacks, leading to a variation in the charge pattern. The shape of the AO anomaly seems to be related to the difference in the coupling between anions and TMTTF stacks.

ACKNOWLEDGMENTS

We thank B. W. Fravel, L. Montgomery, and D. Schweitzer for providing the TMTTF molecules for our crystal growth. Valuable discussions with and numerous comments of S. A. Brazovskii, S. Brown, A. Greco, T. Ishiguro, D. Jérome, J. Merino, and J.-P. Pouget are appreciated. The work was supported by the Deutsche Forschungsgemeinschaft.

[1] S. Kagoshima, H. Nagasawa, and T. Sambongi, *One-Dimensional Conductors* (Springer, Berlin, 1988).
[2] M. Dressel, Naturwissenschaften **90**, 337 (2003).
[3] M. Dressel, Naturwissenschaften **94**, 527 (2007).
[4] D. Jérome and H. J. Schulz, Adv. Phys. **31**, 299 (1982).
[5] D. Jérome, in *Organic Conductors*, edited by J.-P. Farges (Dekker, New York, 1994), p. 405.
[6] T. Ishiguro, K. Yamaji, and G. Saito, *Organic Superconductors*, 2nd ed. (Springer-Verlag, Berlin, 1998).
[7] J. P. Pouget and S. Ravy, J. Phys. (Paris) I **6**, 1501 (1996).
[8] S. A. Brazovskii, in *Ferroelectricity and Charge Ordering in Quasi-1D Organic Conductors*, edited by A. G. Lebed, The Physics of Organic Superconductors and Conductors (Springer-Verlag, Berlin, 2008), p. 313.
[9] M. Dressel, P. Hesse, S. Kirchner, G. Untereiner, M. Dumm, J. Hemberger, A. Loidl, and L. Montgomery, Synth. Met. **120**, 719 (2001).
[10] B. Korin-Hamzić, E. Tafra, M. Basletić, A. Hamzić, and M. Dressel, Phys. Rev. B **73**, 115102 (2006).
[11] C. Coulon, P. Delhaes, S. Flandrois, R. Lagnier, E. Bonjour, and J. M. Fabre, J. Phys. (Paris) **43**, 1059 (1982).
[12] R. Moret, J. P. Pouget, R. Comes, and K. Bechgaard, J. Phys. (Paris) **44**, C3-957 (1983).
[13] J. P. Pouget, R. Moret, R. Comes, K. Bechgaard, J. M. Fabre, and L. Giral, Mol. Cryst. Liq. Cryst. **79**, 129 (1982).
[14] S. Ravy, R. Moret, J. P. Pouget, and R. Comes, Synth. Met. **13**, 63 (1986).
[15] F. Nad and P. Monceau, J. Phys. Soc. Jpn. **75**, 051005 (2006).
[16] G. Mihály, I. Kézsmárki, F. Zámborszky, and L. Forró, Phys. Rev. Lett. **84**, 2670 (2000).
[17] E. Rose, M. Dumm, and M. Dressel (to be published).
[18] N. F. Mott and E. Davies, *Electronic Processes in Non-Crystalline Materials* (Oxford University Press, Oxford, 1979).
[19] A. L. Efros and B. I. Shklovskii, J. Phys. C **8**, L49 (1975); B. I. Shklovskii and A. L. Efros, *Electronic Properties of Doped Semiconductors* (Springer, Berlin, 1984).
[20] T. Takahashi, Y. Nogami, and K. Yakushi, J. Phys. Soc. Jpn. **75**, 051008 (2006).
[21] Note that it is also compatible with an expectation of Brazovskii[8] that the transport is carried out by (spinless) solitons, i.e., holons. As topological objects, the solitons need pair collisions or annihilations to travel between chains.
[22] A. Georges, T. Giamarchi, and N. Sandler, Phys. Rev. B **61**, 16393 (2000).
[23] T. Ishiguro, H. Sumi, S. Kagoshima, K. Kajimura, and H. Anzai, J. Phys. Soc. Jpn. **48**, 456 (1980).
[24] G. Soda, D. Jérome, M. Weger, J. Alizon, J. Gallice, H. Robert, J. M. Fabre, and L. Giral, J. Phys. (Paris) **38**, 931 (1977).
[25] C. S. Jacobsen, D. B. Tanner, and K. Bechgaard, Phys. Rev. Lett. **46**, 1142 (1981).
[26] V. Vescoli, L. Degiorgi, W. Henderson, G. Grüner, K. P. Starkey, and L. K. Montgomery, Science **281**, 1181 (1998).
[27] A. Pashkin, M. Dressel, and C. A. Kuntscher, Phys. Rev. B **74**, 165118 (2006).
[28] A. Pashkin, M. Dressel, M. Hanfland, and C. A. Kuntscher, Phys. Rev. B **81**, 125109 (2010).
[29] T. Granier, B. Gallois, L. Ducasse, A. Fritsch, and A. Filhol, Synth. Met. **24**, 343 (1988).
[30] C. Bourbonnais and D. Jerome, in *The Physics of Organic Superconductors and Conductors*, edited by A. Lebed (Springer-Verlag, Berlin 2008), p. 375.

[31]J. M. Williams, M. A. Beno, H.-H. Wang, T. J. Emge, P. T. Copps, L. N. Hall, K. D. Carlson, and G. W. Crabtree, Philos. Trans. R. Soc. London, Ser. A **314**, 83 (1985).
[32]V. J. Emery, J. Phys. (Paris) **44**, C3-977 (1983).
[33]T. Giamarchi, Physica B **230–232**, 975 (1997); in *From Luttinger to Fermi Liquids in Organic Conductors*, edited by A. Lebed, The Physics of Organic Superconductors and Conductors (Springer-Verlag, Berlin 2007), p. 719.
[34]J. L. Galigné, B. Liautard, S. Peytavin, G. Brun, M. Maurin, J. M. Fabre, E. Torreilles, and L. Giral, Acta Crystallogr., Sect. B: Structual Science **35**, 1129 (1979).
[35]B. Liautard, S. Peytavin, G. Brun, D. Chasseau, J. M. Fabre, and L. Giral, Acta Crystallogr., Sect. C: Cryst. Struct. Commun. **40**, 1023 (1984).
[36]H. Kobayashi, A. Kobayashi, Y. Sasaki, G. Saito, and H. Inokuchi, Bull. Chem. Soc. Jpn. **57**, 2025 (1984); there seems to be a typing error in the unit-cell data: $\alpha = 82.66^\circ$ (instead of 86.62°) is in agreement with other measurements (e.g., Ref. 62) and fits to the unit-cell volume of $V = 679.5$ Å^3 published in the paper. The stacking distances of the molecules along the a direction extracted from the corresponding file are as follows: $d_1 = 3.615$ Å and $d_2 = 3.537$ Å and, thus, differ from those mentioned in the publication.
[37]F. Iwase, K. Sugiura, K. Furukawa, and T. Nakamura, J. Phys. Soc. Jpn. **78**, 104717 (2009).
[38]B. Liautard, S. Peytavin, G. Brun, and M. Maurin, Cryst. Struct. Commun. C **11**, 1841 (1982).
[39]R. Laversanne, C. Coulon, B. Gallois, J. P. Pouget, and R. Moret, J. Phys. Lett. (Paris) **45**, L-393 (1984).
[40]B. Salameh, S. Yasin, M. Dumm, M. Untereiner, L. Montgomery, and M. Dressel, Phys. Rev. B **83**, 205126 (2011).
[41]D. S. Chow, F. Zamborszky, B. Alavi, D. J. Tantillo, A. Baur, C. A. Merlic, and S. E. Brown, Phys. Rev. Lett. **85**, 1698 (2000).
[42]F. Zamborszky, W. Yu, W. Raas, S. E. Brown, B. Alavi, C. A. Merlic, and A. Baur, Phys. Rev. B **66**, 081103 (2002).
[43]F. Y. Nad, P. Monceau, C. Carcel, and J. M. Fabre, Phys. Rev. B **62**, 1753 (2000).
[44]P. Monceau, F. Y. Nad, and S. Brazovskii, Phys. Rev. Lett. **86**, 4080 (2001).
[45]M. Dumm, M. Abaker, and M. Dressel, J. Phys. (Paris) IV **131**, 55 (2005); M. Dumm, M. Abaker, M. Dressel, and L. K. Montgomery, J. Low Temp. Phys. **142**, 609 (2006).
[46]S. Hirose, A. Kawamoto, N. Matsunaga, K. Nomura, K. Yamamoto, and K. Yakushi, Phys. Rev. B **81**, 205107 (2010).
[47]T. Nakamura, K. Furukawa, and T. Hara, J. Phys. Soc. Jpn. **76**, 064715 (2007).
[48]C. Coulon, S. S. P. Parkin, and R. Laversanne, Phys. Rev. B **31**, 3583 (1985).
[49]Y. Nogami and T. Nakamura, J. Phys. (Paris) IV **12**, 9 (2002).
[50]Y. Nogami, T. Ito, K. Yamamoto, N. Irie, S. Horita, T. Kambe, N. Nagao, K. Oshima, N. Ikeda, and T. Nakamura, J. Phys. (Paris) IV **131**, 39 (2005).
[51]L. Ducasse, M. Abderrabba, J. Hoarau, M. Pesquer, B. Gallois, and J. Gaultier, J. Phys. C **19**, 3805 (1986); L. Ducasse, M. Abderrabba, B. Gallois, and D. Chasseau, Synth. Met. **19**, 327 (1987).
[52]M. de Souza, P. Foury-Leylekian, A. Moradpour, J. P. Pouget, and M. Lang, Phys. Rev. Lett. **101**, 216403 (2008); M. de Souza, A. Brühl, J. Müller, P. Foury-Leylekian, A. Moradpour, J.-P. Pouget, and M. Lang, Physica B **404**, 494 (2009); M. de Souza, D. Hofmann, P. Foury-Leylekian, A. Moradpour, J. P. Pouget, and M. Lang, Physica B Suppl. 1 **405**, S92 (2010).
[53]D. P. Pouget in *Low-Dimensional Conductors and Superconductors*, edited by D. Jerome and L. G. Caron (NATO ASI Series, Series B: Physics Plenum, New York, 1986), Vol. 155, p. 38.
[54]P. Foury-Leylekian, S. Petit, G. Andre, A. Moradpour, and J.-P. Pouget, Physica B Suppl. 1 **405**, S95 (2010).
[55]It is particularly fortunate that, for $(TMTTF)_2X$, the more common $4k_F$ instability (CO) coincides with the cagelike setting for the anions. The latter is prone to Earnshaw's instability for all classical charges; for small anions, it may not be stabilized by the rigidity of the methyl groups constituting the cage.
[56]K. Furukawa, T. Hara, and T. Nakamura, J. Phys. Soc. Jpn. **78**, 104713 (2009).
[57]Sometimes the extracted energy gaps deviate beyond the error bars; this can only partially be attributed to different samples and contact quality.
[58]S. A. Brazovskii and N. N. Kirova, JETP Lett. **33**, 4 (1981).
[59]S. A. Brazovskii and V. M. Yakovenko, J. Phys. Lett. (France) **46**, L111 (1985); Sov. Phys. JETP **62**, 1340 (1985).
[60]C. Coulon, A. Maaroufi, J. Amiell, E. Dupart, S. Flandrois, P. Delhaes, R. Moret, J. P. Pouget, and J. P. Morand, Phys. Rev. B **26**, 6322 (1982); C. Coulon, P. Delhaes, S. Flandrois, R. Lagnier, E. Bonjour, and J. M. Fabre, J. Phys. (Paris) **43**, 1059 (1982).
[61]M. Dumm, A. Loidl, B. W. Fravel, K. P. Starkey, L. K. Montgomery, and M. Dressel, Phys. Rev. B **61**, 511 (2000); M. Dumm, B. Salameh, M. Abaker, L. K. Montgomery, and M. Dressel, J. Phys. (Paris) IV **114**, 57 (2004).
[62]K. Furukawa, T. Hara, and T. Nakamura, J. Phys. Soc. Jpn. **74**, 3288 (2005).